Synthesis and 3D Network Architecture of 1- and 16-Hydrated Salts of 4-Dimethylaminopyridinium Decavanadate, (DMAPH)$_6$[V$_{10}$O$_{28}$]·nH$_2$O

Eduardo Sánchez-Lara [1], Aarón Pérez-Benítez [2], Samuel Treviño [2], Angel Mendoza [1], Francisco J. Meléndez [2], Enrique Sánchez-Mora [3], Sylvain Bernès [3] and Enrique González-Vergara [1,*]

[1] Centro de Química del Instituto de Ciencias, Benemérita Universidad Autónoma de Puebla, 18 sur y Av. San Claudio, Col. San Manuel, C. P. 72570 Puebla, Mexico; esl_24@hotmail.com (E.S.-L.); angel.mendoza.m@gmail.com (A.M.)

[2] Facultad de Ciencias Químicas, Benemérita Universidad Autónoma de Puebla, 18 sur y Av. San Claudio, Col. San Manuel, C. P. 72570 Puebla, Mexico; aaron.perez@correo.buap.mx (A.P.-B.); samuel_trevino@hotmail.com (S.T.); francisco.melendez@correo.buap.mx (F.J.M.)

[3] Instituto de Física, Benemérita Universidad Autónoma de Puebla, Apdo. Postal J-48, C. P. 72570 Puebla, Mexico; esanchez@ifuap.buap.mx (E.S.-M.); sylvain_bernes@hotmail.com (S.B.)

* Correspondence: enrique.gonzalez@correo.buap.mx; Tel.: +52-222-2295500

Abstract: Two hybrid materials based on decavanadates (DMAPH)$_6$[V$_{10}$O$_{28}$]·H$_2$O, (**1**) and (DMAPH)$_6$[V$_{10}$O$_{28}$]·16H$_2$O, (**2**) (where DMAPH = 4-dimethylaminopyridinium) were obtained by reactions under mild conditions at T = 294 and 283 K, respectively. These compounds are pseudopolymorphs, which crystallize in monoclinic $P2_1/n$ and triclinic $P\bar{1}$ space groups. The structural analysis revealed that in both compounds, six cations DMAPH interact with decavanadate anion through N-H···O$_{dec}$ hydrogen bonds; in **2**, the hydrogen-bonding association of sixteen lattice water molecules leads to the formation of an unusual network stabilized by decavanadate clusters; this hydrogen-bond connectivity is described using graph set notation. Compound **2** differs basically in the water content which in turn increases the π···π interactions coming from pyridinium rings. Elemental and thermal analysis (TGA/DSC) as well as FT-IR, FT-Raman, for **1** and **2** are consistent with both structures and are also presented.

Keywords: hybrid decavanadates; water cluster network; crystal structure; vibrational spectroscopy

1. Introduction

Within the large family of polyoxovanadates, decavanadate anion, [V$_{10}$O$_{28}$]$^{6-}$, is one of the most common and most stable V(V) oxo-clusters found in the acidic pH range [1] and it has been recognized as a chemical specie with great biological interest [2–5]. Decavanadate can be found in different protonation states, [H$_n$V$_{10}$O$_{28}$]$^{(6-n)-}$, in which n can vary from 1 to 4 depending on the chemical nature of the counterion and the acidity range of media [6–10]. In the cluster [V$_{10}$O$_{28}$]$^{6-}$, ten vanadium atoms and 28 oxygen atoms are arranged in a highly condensed system of VO$_6$ octahedra.

It may be described as a group of six VO$_6$ octahedra arranged in a 2 × 3 rectangular array by sharing edges, with two VO$_6$ octahedra joined from above and two more from below by sharing sloping edges with the central six octahedra. The structure conforms closely to an ideal arrangement with orthorhombic symmetry mmm [10].

A second approach of interest in this field is the study of non-covalent interactions arising from the electrostatic Coulomb attractive forces between decavanadate and suitable cationic organic, inorganic,

or biological molecules (*i.e.*, peptides or proteins) [11–15]. The study of those interactions in the solid state could give us more information on both the cooperative effects of decavanadate in biological systems [16] and its influence in the crystal packing and the dimensional arrays that are produced due to its stereochemistry. Special attention has been paid in establishing how the nature, size, and shape of the cation(s) and solvent(s), as well as the degree and site(s) of protonation(s) of decavanadate, are essential for forming a fascinating variety of supramolecular assemblies [17–20]. In those materials, the decavanadate acts as an excellent acceptor of protons coming from proton-donor functional groups such as amines, phosphines [19,21], *etc.*, producing hydrogen bond interactions $X-H\cdots O_{dec}$ (where X = N, P, O, C, *etc.*) that function as a cement for building the 3D crystal network.

Because of the steric effect of decavanadate and/or due to the presence of bulk counter-cations and/or for stabilizing small metal cations (*i.e.*, $Na(H_2O)_6^+$, $Co(H_2O)_6^+$), a great number of decavanadate-based materials add water into their structures thereby generating different kinds of hydrated species, even starting from the same reaction conditions or when the temperature of crystallization is changed [22]. This approach favors our interest in the search of new types of supramolecular arrangements and for developing new synthetic methodologies for seeking them.

The first attempt to obtain a compound based on $[V_{10}O_{28}]^{6-}$ units and 4-dimethylaminopyridine (4-DMAP) was explored by our group and, as a result, we obtained a hybrid dicationic salt of formula: $[DMAPH]_4[NH_4]_2[V_{10}O_{28}]\cdot 8H_2O$ [23]. With the purpose of replacing the NH_4^+ ions to get new 3D architectures, the starting material NH_4VO_3 was replaced by KVO_3. *A priori*, we expected that K^+ ions were present in the crystal structure in the form of aquocomplexes as those mentioned above [18,24,25]; however, DMAPH cations were incorporated in the resulting materials and water molecules were occluded during the crystallization processes at different temperatures to yield $[DMAPH]_6[V_{10}O_{28}]\cdot H_2O$ (**1**) and $[DMAPH]_6[V_{10}O_{28}]\cdot 16H_2O$ (**2**).

On the other hand, Wu B. *et al.* reported very recently the synthesis and X-ray structure of **2** following an experimental procedure a little more complicated than the one presented here; however, the physical and chemical aspects and even important crystallographic data of this crystalline material were missed [26]. Bearing in mind this fact, the goal of the present study is to give a complete description of the molecular structure of **1** and **2** for the first time.

2. Results and Discussion

2.1. Features of Crystalline Structures of *1 and 2*

Compound **1** crystallizes at 294 K with low water content. The formula, as determined by X-ray diffraction, is $(DMAPH)_6[V_{10}O_{28}]\cdot H_2O$, with the decavanadate placed on an inversion center and the water molecule occupying a general position, with an occupancy factor best refined to 1/2. Six DMAPH cations are in close contact with the decavanadate through $N–H\cdots O_{dec}$ hydrogen bonds with µ2- and µ3-O sites of the anion (Figure 1). These interactions clearly belong to the class of strong hydrogen bonds, with $H\cdots O_{dec}$ distances in the range of 1.71(2)–1.75(2) Å and $N–H\cdots O_{dec}$ angles of 180°, if one takes into account the standard deviations for these parameters (Table 1). The $\pi\cdots\pi$ interactions in the crystal (Figure 1, inset) are disrupted. Significant interactions are thus limited to independent $(DMAPH)_6[V_{10}O_{28}]$ entities. In the asymmetric unit, only N1- and N21-based DMAPH cations generate a $\pi\cdots\pi$ contact, characterized by the centroid-to-centroid distance of 3.66 Å and a tilt angle of 14.4(2)°. The third independent DMAPH cation (N11) does not participate in any such stabilizing contact.
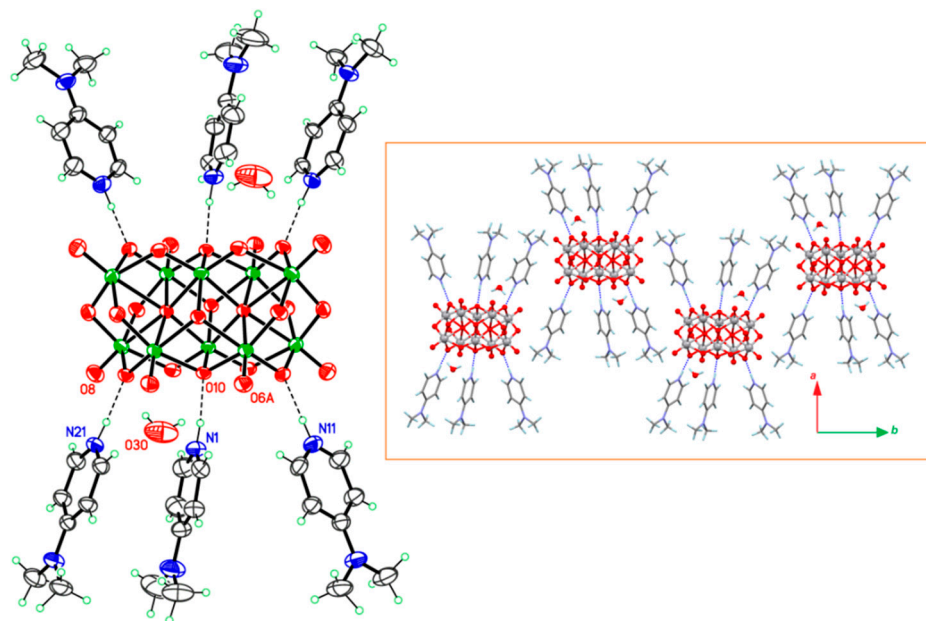
Figure 1. Structure of compound **1**, (DMAPH)$_6$[V$_{10}$O$_{28}$]· H$_2$O, with displacement ellipsoids shown at the 50% probability level. Hydrogen bonds linking cations and anions are represented by dashed lines. The site occupation factor for the water molecule O30 is 1/2. The inset displays the arrangement of clusters in the crystal [27].

Table 1. Hydrogen bonds in the crystal structure of **1**, (HDMAP)$_6$[V$_{10}$O$_{28}$]·H$_2$O.

H bond D–H$\cdots A$	H$\cdots A$ (Å)	D–H$\cdots A$ (°)	Symmetry for A
Interactions DMAPH/[V$_{10}$O$_{28}$]			
N1–H1$\cdots$O10	1.71 (2)	174 (4)	x, y, z
N11–H11$\cdots$O6	1.721 (19)	179 (4)	$1 - x, 1 - y, 2 - z$
N21–H21$\cdots$O8	1.754 (19)	175 (4)	x, y, z

Although the orientation of the single water molecule present in the asymmetric unit was determined from difference maps, this molecule is not engaged in hydrogen bonding and, as a consequence, the crystal structure of **1** has no supramolecular features. It may be inferred that the (DMAPH)$_6$[V$_{10}$O$_{28}$] heterostructure found in **1** is tightly assembled by both Coulombic forces and hydrogen bonds. Assuming that this structure survives in solution, it may be seen as a direct precursor of **2**, obtained by hydration of **1**. There may be several stable intermediates with formulas (DMAPH)$_6$[V$_{10}$O$_{28}$]· nH$_2$O ($1 < n < 16$) which could be crystallized, but the end hydrates obtained in this study, with $n = 1$ and $n = 16$, seem to be very stable. On the other hand, equilibrated hydration reactions should not be ruled out and the possibility of formation of **1** starting from **2** under certain circumstances may be envisaged, too.

Compound **2**, (DMAPH)$_6$[V$_{10}$O$_{28}$]·16H$_2$O, crystallizes in a triclinic cell, with the decavanadate anion [V$_{10}$O$_{28}$]$^{6-}$ lying over an inversion center, while three independent DMAPH cations and eight water molecules are placed in general positions (Figure 2 [27]). No evidence for disorder affecting water positions was observed during the model refinement, as reflected in homogeneous displacement parameters for these molecules. The residual electronic density is actually low for room-temperature data, *ca.* 0.40 e-/Å^3, and the quality of X-ray diffraction data was sufficiently high to determine the accurate orientation of all water molecules, for which H atoms were clearly visible in difference maps, as well as H atoms in protonated DMAPH fragments. The resulting crystal structure may be considered to be a very efficient aggregation state, as evidenced by the high packing index of the crystal, $C_k = 0.722$ [28].
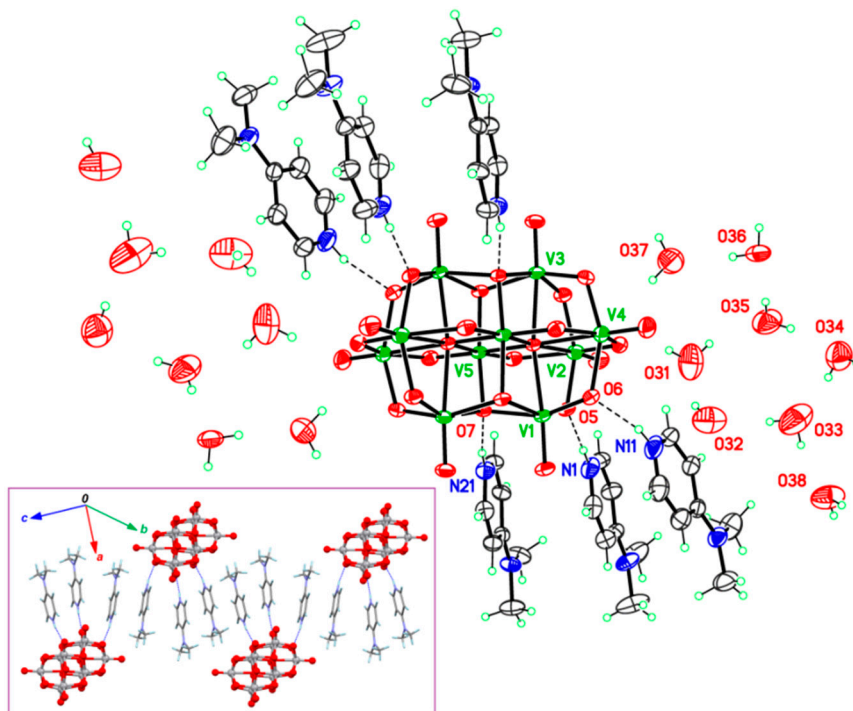
Figure 2. The unit cell contents of compound **2**, (DMAPH)$_6$[V$_{10}$O$_{28}$]· 16H$_2$O. Displacement ellipsoids were drawn at the 50% probability level. Main atoms were labeled in the asymmetric unit, and the complete cell is generated by symmetry code $2 - x$, $2 - y$, $2 - z$. The dashed lines represent H bonds between cations and anions. The inset represents a part of the crystal structure, omitting all lattice water molecules [27]. The orientation for this projection evidences the stacking of cations in the crystal.

The three independent cations of DMAPH strongly interact with [V$_{10}$O$_{28}$]$^{6-}$ via N–H···O$_{dec}$ hydrogen bonds involving the protonated pyridine rings as donor groups and three oxo groups of the decavanadate as acceptors (Figure 2 and Table 2). Each anion in the crystal is thus encapsulated by six cations, forming a stable, neutral entity. This result is confirmed by the bond valence sum calculations for [V$_{10}$O$_{28}$]$^{6-}$, which is consistent with formal V^{5+} sites [29]: BVS for the five independent V sites are in the range 5.05–5.09 v.u. More stability is achieved through the arrangement of these components in the crystal, in a way affording almost perfect stacks of cations oriented in the $[01\,\overline{1}]$ direction (see Figure 2, inset). Pyridine π-systems are nearly parallel along a stack and π···π separations, ranging from 3.58 to 3.89 Å, are short enough to ensure strong stabilizing interactions [30]. This effective packing is favored by the planar character of the DMAPH cation, previously observed in many salts, as chloride [31,32], picrate [33], or perchlorate [34], among others.

The (DMAPH)$_6$[V$_{10}$O$_{28}$] association affords an anisotropic entity, which, once packed in the triclinic crystal, left *ca.* 20% of the unit-cell volume empty. These voids are filled by water molecules, giving a highly hydrated formula, with a ratio water/POV (polyoxovanadate) = 16. A scan of the CSD [35] shows that the most hydrated [V$_{10}$O$_{28}$]-based structures reported to date have formulas with water/POV = 20 [36], and water/POV = 15 [37]. Both compounds feature complex hydrogen bonds schemes for water molecules, although their graph sets remain fuzzy, because water H atoms were not localized in the former structure and the disorder affects water sites in the latter. In contrast, in compound **2**, the supramolecular structure formed by water molecules is clearly defined.

Table 2. Hydrogen bonds in the crystal structure of **2**.

H bond D–H $\ldots$ A	H $\ldots$ A (Å)	D–H $\ldots$ A (°)	Symmetry for A
Interactions DMAPH/[V$_{10}$O$_{28}$]			
N1–H1$\cdots$O5	1.94 (3)	170 (3)	x, y, z
N11–H11$\cdots$O6	1.97 (3)	166 (3)	x, y, z
N21–H21$\cdots$O7	1.94 (3)	168 (3)	x, y, z
Interactions H$_2$O/H$_2$O building the C [R (10) R (12)] network			
O31–H31B$\cdots$O35	1.98 (3)	153 (6)	x, y, z
O32–H32B$\cdots$O31	1.99 (3)	151 (5)	x, y, z
O33–H33A$\cdots$O32	1.99 (2)	173 (6)	x, y, z
O33–H33B$\cdots$O38	1.92 (2)	164 (5)	x, y, z
O34–H34A$\cdots$O36	2.10 (2)	160 (5)	$1 - x, 3 - y, 1 - z$
O34–H34B$\cdots$O33	1.94 (2)	168 (5)	x, y, z
O35–H35A$\cdots$O36	1.959 (18)	177 (5)	x, y, z
O35–H35B$\cdots$O34	1.96 (2)	164 (5)	x, y, z
O36–H36B$\cdots$O37	1.94 (2)	166 (3)	x, y, z
O38–H38A$\cdots$O32	2.19 (2)	162 (5)	$-x, 2 - y, 1 - z$
Interactions H$_2$O/[V$_{10}$O$_{28}$]			
O31–H31A$\cdots$O2	2.28 (3)	141 (4)	x, y, z
O32–H32A$\cdots$O13	2.11 (2)	166 (5)	$-1 + x, y, z$
O36–H36A$\cdots$O1	1.948 (18)	178 (3)	$x, 1 + y, z$
O37–H37A$\cdots$O12	2.31 (2)	163 (5)	x, y, z
O37–H37B$\cdots$O3	2.25 (3)	144 (4)	$2 - x, 3 - y, 2 - z$
O38–H38B$\cdots$O6	1.96 (2)	173 (5)	$1 - x, 2 - y, 1 - z$

Water molecules O31 to O35 form a ring motif R_5^5 (10) [38] in which five non-symmetry related hydrogen bonds are involved. In other words, this motif is a fifth-level supramolecular structure, characterized by a constructor graph based on the oriented path $R(\overleftarrow{a}\,\overleftarrow{b}\,\overleftarrow{c}\,\overleftarrow{d}\,\overleftarrow{e})$, according to the Samuel Motherwell's nomenclature [39]. This ring is edge-fused with two larger R_6^4 (12) centrosymmetric rings involving each six water molecules: O34, O35, O36, O34^i, O35^i, and O36^i (symmetry code i: $1 - x$, $3 - y$, $1 - z$) for the first one, and O32, O33, O38, O32^{ii}, O33^{ii}, and O38^{ii} (symmetry code ii: $-x$, $2 - y$, $1 - z$) for the other. Both six-membered rings are third-level R_6^4 (12) motifs, although they are not identical from the graph-set point of view, because different sets of hydrogen bonds are involved. Corresponding paths may be described as $R(\overrightarrow{a}\,\overrightarrow{f}\,\overleftarrow{g}\,\overrightarrow{a}\,\overrightarrow{f}\,\overleftarrow{g})$ and $R(\overrightarrow{d}\,\overleftarrow{h}\,\overrightarrow{i}\,\overrightarrow{d}\,\overleftarrow{h}\,\overleftarrow{i})$, where H-bond types a and d are the graph edges fusing 5- and 6-membered rings (see Figure 3). Ring R_5^5 (10) is flat, while a slight puckering is observed for R_6^4 (12) rings, which adopt a chair conformation. All hydrogen bonds have a significant strength and should thus participate in the global stabilization of the solid state structure. The ranges for H$\cdots$O$_{dec}$ separations and O–H$\cdots$O$_w$ angles are 1.92(2)–2.19(2) Å and 151(5)–177(5)°, respectively (Table 2).

The resulting rings network is extended in the [110] direction, forming a serpent like undulating structure (Figure 2, green bonds) with the graph set descriptor $C\left[R_5^5 (10)\, R_6^4 (12)\right]$. This backbone alternating 5- and 6-membered rings is rather uncommon in hydrated crystals, even if pentagonal and hexagonal arrangements of water molecules are ubiquitous in hydrates. Apparently, very few crystal structures presenting a supramolecular arrangement for lattice water molecules similar to that observed in **2** are available to date. Moreover, the search for similar networks is impaired by the high level of the R_5^5 (10) ring in **2**, since no software is currently available for retrieving ring systems with a complexity above the fourth level [28]. However, we have found at least one example of a C [R (10) R (12)] network for water molecules in the tri-hydrate of a pyridine derivative [40]. In that case, five membered rings are fourth level R_5^4 (10) motifs with an envelope conformation, and the six membered rings are third level R_6^6 (12) centrosymmetric motifs with a chair conformation, similar to that observed for **2**. The topology of the chain structure of fused rings, C [R (10) R (12)], is the same in this pyridinyl derivative and in **2**, but H-bond paths in individual rings are different.

In crystals of **2**, the chains of rings are further connected to the $[V_{10}O_{28}]^{6-}$ clusters by means of secondary hydrogen bonds with cluster O atoms as acceptor groups (Figure 3, blue bonds; Table 2). New rings are formed, with descriptors R_3^3 (8), R_3^3 (10) , and R_5^5 (12). All water molecules in the crystal serve both as donors and acceptors to form the whole supramolecular network of hydrogen bonds.
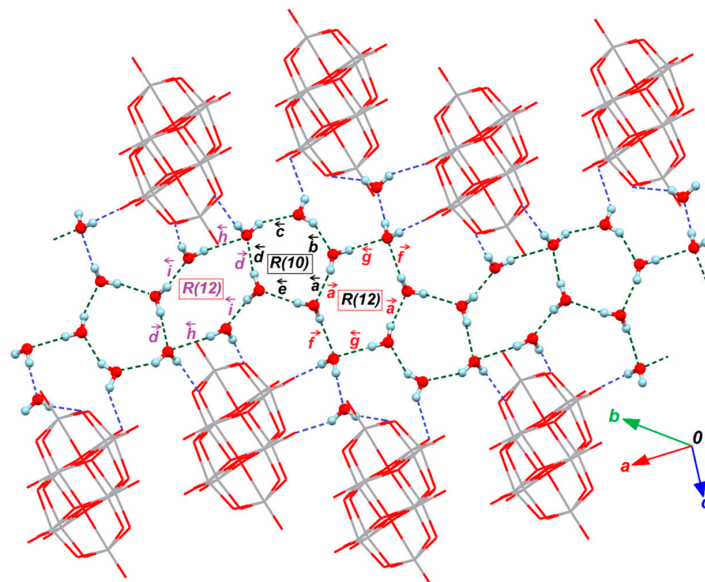

Figure 3. A part of the crystal structure of **2**, omitting cations. The supramolecular network formed by water molecules were based on hydrogen bonds (dashed lines, [27]). Blue H-bonds were used to form the $C[R(10)R(12)]$ backbone, in which R_5^5 (10) and R_6^4 (12) rings alternate. The different types of H-bonds were labeled $a - i$ and ring sequences are oriented counter-clockwise. Blue H-bonds connect this backbone to $[V_{10}O_{28}]^{6-}$ anions in the crystal.

Crystallographic data are summarized in Table 3.

Table 3. Selected crystal data and details of the structure determination for the two compounds.

	Compound 1	Compound 2
Empirical formula	$C_{42}H_{68}N_{12}O_{29}V_{10}$	$C_{42}H_{98}N_{12}O_{44}V_{10}$
Formula weight	1714.48	1984.72
Crystal system	Monoclinic	Triclinic
T [K]	298 (2)	283 (2)
Wavelength, λ/Å	Cu-K_α,1.5418	Mo-K_α, 0.71073
Space group	$P2_1/n$	$P\bar{1}$
a [Å]	11.0212 (2)	11.2785 (3)
b [Å]	23.845 (4)	11.7777 (3)
c [Å]	12.20887 (19)	15.0569 (4)
α	90	93.4088 (19)
β	103.3414 (17)	102.469 (2)
γ	90	100.691 (2)
V [Å^3]	3122.0 (5)	1908.65 (9)
Z	2	1
$D_{calc.}$ [g/cm^3]	1.824	1.727
μ [mm^{-1}]	12.794	1.268
Reflections collected	42521	42872
Independent reflections	5572	9716
Parameters	445	555
Goodness-of-fit on F^2	1.047	1.039
Final R index [$I > 2\sigma(I)$]	0.042	0.033
wR_2 (all data)	0.127	0.092

2.2. FT-IR and FT-Raman Spectroscopic Studies

The middle infrared and Raman spectra of **1** and **2**, and neutral 4-DMAP are provided in Figure 4 and summarized in Table 4. In general, the IR spectra of both materials are quite similar because of the same chemical components; however, the lattice water absorption bands centered at 3400 and 3200 cm^{-1} are more intense in **2** than in **1**, which is in agreement with its major water content. These bands have been attributed to asymmetric and symmetric H-O-H stretching vibration modes [41] and they must be overlapped with other stretching bands coming from N^+–H$\cdots O_{dec}$ and O_w–H$\cdots O_{dec}$ moieties. In the same spectra, the bands at 3050 and 2900 cm^{-1} are respectively assigned to the (C–H)$_{aromatic}$ and (C–H)$_{aliphatic}$ stretching vibrations [42].
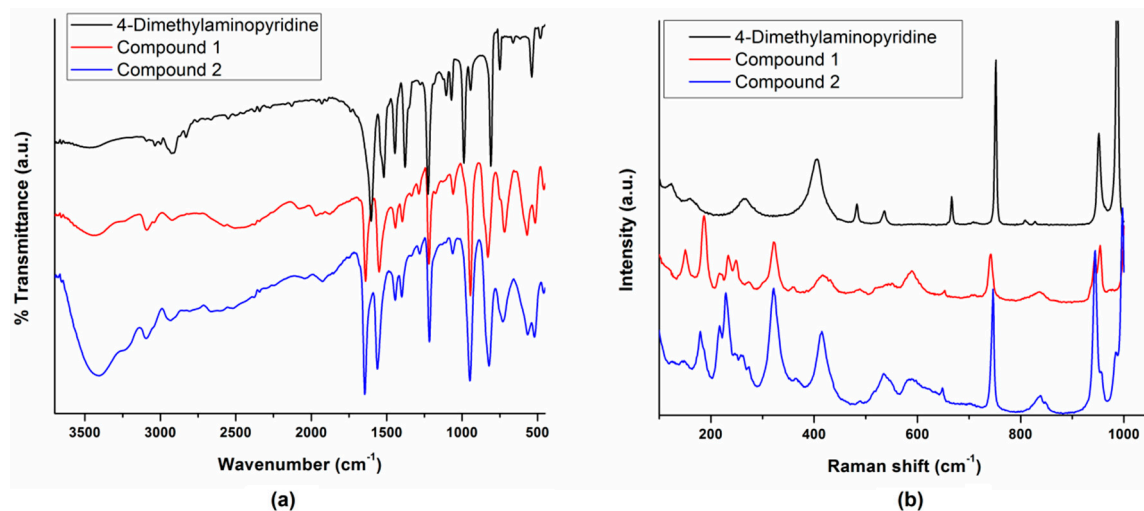

Figure 4. FT-IR (**a**) and Raman spectra (**b**) of 4-dimethylaminopyridine and their corresponding hydrated decavanadate salts **1** and **2**, (**a**) recorded in KBr pellets.

The carbon C=C aromatic stretch, known as semicircle stretching, shows an intense peak at 1640 cm^{-1}. The bands at 1540 and 1440 cm^{-1} are ascribed to the stretching vibrations C=N and C–N, respectively [43]. The weak band at 1398 and the strong band at 1220 cm^{-1} are due to in-plane C–H bending. The spectra of **1** and **2** display the terminal V=O$_t$ stretching bands within the range 1000–950 cm^{-1}. The corresponding vibrations for **1** and **2** appear in the Raman spectrum at 953 and 943 cm^{-1}, respectively, with strong intensities [44,45].

The two high-intensity bands in the range of 820–732 cm^{-1} of the FT-IR correspond to asymmetric vibration mode bridge V-O$_b$ [45]. An important fact here is that slight displacements in **1** and **2** indicate that the anion $[V_{10}O_{28}]^{6-}$ is slightly affected by the amount of water present in both structures. The asymmetric and symmetric bridging vibrations of V$-$O$_b$ in the Raman spectrum appear in the range of 840–741 cm^{-1}, respectively. However, these signals are overlapping with the CNC in plane bending vibrations of the HDMAP cations. The bands observed at 650 and 415 cm^{-1} in FT-Raman are assigned to CCC deformation of pyridine ring [43]. The asymmetric stretching of V_2O_2 and bending of VO_3 units are recorded in the 590 cm^{-1} region. In FT-IR spectrum signs around 400 cm^{-1} for the two compounds are attributed to deformation vibration of the groups V$-$O$_b$. The frequencies observed in FT-Raman spectrum in the range 364–250 cm^{-1} may be attributed to the V$-$O$_b$ bending modes and bending of VO_3 units. Bands below 240 cm^{-1} are attributed to V$-$O bonds and lattice vibrations [46,47].

Table 4. Assignments of the IR and Raman absorption bands for **1**, **2**, and 4-DMAP [42–47].

Compound 1		Compound 2		4-DMAP		
FT-IR [a] (cm^{-1})	FT-Raman (cm^{-1})	FT-IR (cm^{-1})	FT-Raman (cm^{-1})	FT-IR (cm^{-1})	FT-Raman (cm^{-1})	Vibrational Assignment [b]
3440 vw		3416 vbr				ν (O-H) + O-H$\cdots$H stretch
3090 w		3092 w		3092 vw		ν_sCH
3041 vw		3043 vw		3034 vw		ν_s CH
2923 vw		2932 vw		2919 w		ν_{as} CH in CH$_3$
1640 vs		1645 vs		1603 vs		ν. C=C
1550 s		1561 s		1519 s		ν C=C + ν C=N
1443 w		1444 w		1445 s		ν C=N
1395 w		1400 w		1378 w		CH$_3$ umbrella mode + ν C=C
1220 s		1217 s		1225 w		β CH
1059 vw		1062 vw		1071 w		ρ CH$_3$
	1000 vs		997 vs	988 vs	986 vs	νV−O$_{terminal}$ + Trigonal bending
945 vs	943 s	948 vs	947 s	943 m	951 s	ν V−O$_{terminal}$ + Ring breathing + methyl rocking
829 s	837 w	821 vs	837 vw	809 s	808 w	ν_{as} (O−V$_2$) + γCH
719 m	741 vs	728 m	745 vs	750 m	752 vs	ν_{as} (O−V$_2$) + βCNC + γ CCC
569 m	590 w	566 m	586 w			ν_s (O−V$_2$)
515 m	544 vw	520 m	534 w		538 m	ν_s (O−V$_2$) + β N−CH$_3$ + β CCC
	417 w		413 m		405 m	γ CCC
	322 m		321 s			Bending of VO$_3$ units V−O−V bridging bending modes
	232 m		230 s		159 w	V −O and lattice modes + τ CH$_3$
	216 w		215 m		123 w	
	186 m		180 m			

[a] (s) Strong; (vs) very strong; (m) medium; (w) weak; (vw) very weak; (br) broad; (vbr) very broad;
[b] (ν) stretching; (ν_s) sym. stretching; (ν_{as}) asym. stretching; (β) in-plane-bending; (γ) out-of-plane bending; (ρ) rocking; (τ) torsion.

2.3. Thermal Analysis

The monohydrated compound **1** is stable up to 209 °C (Figure S1). From 210 to 300 °C, the weight loss is *ca.* 30% corresponding to the oxidization of 4-dimethylaminopyridinium cations and the decomposition of the $[V_{10}O_{28}]^{6-}$ cluster. The starting of the weight loss coincides with an endothermic peak in the DSC curve at 220 °C. Thermal behavior of the two hydrates is very similar above 250 °C. IR spectra of intermediaries are observed at 250 and 380 °C and are very similar to those obtained for **1** (Figure S2). Thermogravimetric analysis of compound **2** shows a weight loss of almost 10% that can be attributed to the loss of water molecules. This is lower than the calculated value of 14.52% for the sixteen lattice water molecules, probably due to the evaporation of water before or during the sample preparation (Figure S3). This weight-loss coincides with the endothermic peak in DSC at 70 °C. In the range of 190–350 °C the total weight loss of **2** is 25%. In this stage there is an oxidization of the 4-dimethylaminopyridinium cations and decomposition of $[V_{10}O_{28}]^{6-}$ as can be corroborated by an endothermic peak in the DSC curve at 210 °C. Comparing the IR spectrum of **2** with the intermediate (black amorphous product) obtained at 250 °C (Figure S4) changes in signals of $[V_{10}O_{28}]^{6-}$ cluster can be observed, which is indicating the breakdown of cage and the consequent formation of products possibly containing mixed valence oxides [48–51]. At 340 °C a loss of about 30% occurs for the total sample. The intermediate obtained at 380 °C indicates changes from the specimen heated to 250 °C. The signals ranging from 1000 to 500 cm^{-1} indicate the total collapse of the decavanadate ion and the formation of V_2O_5 with traces of organic particles.

3. **Experimental Section**

All chemicals were analytical reagent grade and purchased from Sigma-Aldrich (Toluca, Mexico). Infrared Spectrum was obtained in KBr pellets from 400 to 4000 cm^{-1} by using an IR Digilab, Mod. Scmitar FT-IR (Varian-Agilent Technologies, Santa Clara, CA, USA). Raman spectra were obtained at

room temperature in backscattering configuration using 633 nm line of a He-Ne laser as excitation source by using a LabRAM HR-Olympus Micro Raman system (Horiba Jobin Yvon Inc. Edison, NJ, USA).

The single-crystal X-ray data were recorded with an Agilent Gemini A diffractometer, software: SHELX-2014/7 [52]. Selected crystal data and details of the structure determination of the compounds are summarized in Table 3. CCDC numbers 1449353 (compound **1**) and 1449352 (compound **2**) contain the supplementary crystallographic data for this paper. These data can be obtained free of charge via http://www.ccdc.cam.ac.uk/conts/retrieving.html (or from the CCDC, 12 Union Road, Cambridge CB2 1EZ, UK; Fax: +44-1223-336-033; E-mail: deposit@ccdc.cam.ac.uk).

Thermogravimetry/differential scanning calorimetry data were obtained by using a Nalitek STA 449 F3 Jupiter thermal analyzer. The TGA plots were recorded in the range 25–700 °C for **1** and 25–500°C for **2** with a heating rate of 10 °C/min under a nitrogen atmosphere. The elemental analyses for **1** and **2** were performed in duplicate at the Instituto de Química, UNAM with a Thermo Scientific analyzer.

*Synthesis of (DMAPH)$_6$[V$_{10}$O$_{28}$]· H$_2$O, (**1**) and (DMAPH)$_6$[V$_{10}$O$_{28}$]· 16H$_2$O (**2**)*

For the synthesis of compound (**1**), two solutions *a* and *b* were mixed. Solution *a* was prepared with 0.5 g (3.62 mmol) of potassium metavanadate (KVO$_3$) dissolved in 30 mL of distilled water; whereas solution *b* contained 0.122 g (1 mmol) of 4-dimethylaminopyridine (4-DMAP) dissolved in 5 mL of distilled water.

The solution *a* was treated with three drops of concentrated hydrochloric acid (37%) to reach a pH~6 and hence the formation of the ion decavanadate [V$_{10}$O$_{28}$]$^{6-}$, which is indicated by the appearance of a bright orange solution. Then, the solution *b* was added dropwise to the orange solution *b*. Finally, this mixture was kept at room temperature for one day to produce orange single crystals needles (Figure 5a). The crude yield was 20% based on vanadium. Anal. Calc. for C$_{42}$H$_{68}$N$_{12}$O$_{29}$V$_{10}$ (MW = 1714.48 g/mol) C, 29.18%; H, 3.99%; N 9.612%. Found: C, 29.39%; H, 3.96%; N, 9.80%.

Compound (**2**) was synthetized as mentioned above, but the mixture of *a+b* was kept at 283 K for one day. The main product consisted of orange single crystal polyhedral bars (Figure 5b). The crude yield was 20% based on vanadium. For this compound inconsistent elemental analysis were obtained due to gradual loss of water molecules and therefore loss of crystallinity.
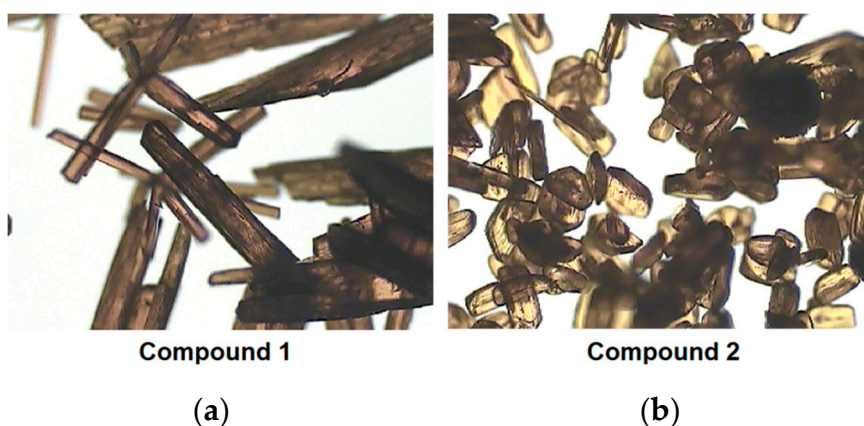

Figure 5.   Images of crystal morphologies observed by optical stereoscopic microscope. (**a**) (DMAPH)$_6$[V$_{10}$O$_{28}$]· H$_2$O; (**b**) (DMAPH)$_6$[V$_{10}$O$_{28}$]· 16H$_2$O.

4. Conclusions

In summary, the results obtained from the study of the reactivity of polyoxovanadate [V$_{10}$O$_{28}$]$^{6-}$ with 4-dimethylaminopyridine are reported. Applying identical starting material ratios but varying the crystallizatin temperature compounds **1** and **2** were obtained. The electrostatic interactions between decavanadate ions and organic cations have been discussed in detail. We have characterized

a well-resolved infinite water cluster chain encapsulated in an organic decavanadate supramolecular framework. This result further enhances the understanding of hydrogen-bonding interactions of water clusters. The IR and Raman spectra confirm the existence of VO_6 octahedra, which is consistent with the results obtained from the single-crystal X-ray structural analysis. Thermal decomposition of both materials suggested the formation of vanadium organic microparticles. Actually, our research points towards the biochemical application of these materials, specifically to their anticancer activity [53].

Supplementary Materials: The following are available online at http://www.mdpi.com/2073-4352/6/6/65/s1, Figure S1: TGA and DTA for **1**, Figure S2: FT-IR spectra of **1**, as prepared sample, and the residue at different temperatures, Figure S3: TGA and DTA for **2**, Figure S4: FT-IR spectra of **2**, as newly synthesized sample, and the residue at different temperatures.

Author Contributions: Eduardo Sánchez-Lara and Aarón Pérez-Benitez carried out experimental work (synthesis, crystallization and characterization), Ángel Mendoza determined the crystal structures and Sylvain Bernès refined and analyzed the crystallographic data. Enrique Sánchez-Mora contributed the Raman measurements. Eduardo Sánchez Lara, Aarón Pérez Benítez, Samuel Treviño, Fransisco J. Meléndez, Sylvain Bernès and Enrique González Vergara wrote and revised the manuscript. Eduardo Sánchez Lara and Enrique Gonzalez Vergara conceived and designed this study. All authors contributed extensively to the work presented in this paper.

Conflicts of Interest: The authors declare no conflict of interest.

Abbreviations

The following abbreviations are used in this manuscript:

DMAP	4-Dimethylaminopyridine
DMAPH	4-Dimethylaminopiridinium
POV	Polyoxovanadate

References and Notes

1. Hayashi, Y. Hetero and lacunary polyoxovanadate chemistry: Synthesis, reactivity and structural aspects. *Coord. Chem. Rev.* **2011**, *255*, 2270–2280. [CrossRef]

2. Aureliano, M.; Ohlin, C.A. Decavanadate *in vitro* and *in vivo* effects: Facts and opinions. *J. Inorg. Biochem.* **2014**, *137*, 123–130. [CrossRef] [PubMed]

3. Aureliano, M.; Crans, D.C. Decavanadate ($V_{10}O_{28}{}^{6-}$) and oxovanadates: Oxometalates with many biological activities. *J. Inorg. Biochem.* **2009**, *103*, 536–546. [CrossRef] [PubMed]

4. Rehder, D. The future of/for vanadium. *Dalton Trans.* **2013**, *42*, 11749–11761. [CrossRef] [PubMed]

5. Pereira, M.J.; Carvalho, E.; Eriksson, J.W.; Crans, D.C.; Aureliano, M. Effects of decavanadate and insulin enhancing vanadium compounds on glucose uptake in isolated rat adipocytes. *J. Inorg. Biochem.* **2009**, *103*, 1687–1692. [CrossRef] [PubMed]

6. Nakamura, S.; Ozeki, T. Hydrogen-bonded aggregates of protonated decavanadate anions in their tetraalkylammonium salts. *J. Chem. Soc. Dalton Trans.* **2001**, *4*, 472–480. [CrossRef]

7. Arrieta, J.M. Total synthesis of decavanadates of organic bases. X-ray crystal structures of four decavanadates. *Polyhedron* **1992**, *11*, 3045–3068. [CrossRef]

8. Kempf, J.Y.; Rohmer, M.M.; Poblet, J.M.; Bo, C.; Benard, M. Relative basicities of the oxygen sites in [V10O28]6-. An analysis of the ab initio determined distributions of the electrostatic potential and of the Laplacian of charge density. *J. Am. Chem. Soc.* **1992**, *114*, 1136–1146. [CrossRef]

9. Day, V.W.; Klemperer, W.G.; Maltbie, D.J. Where are the protons in H3V10O283-? *J. Am. Chem. Soc.* **1987**, *109*, 2991–3002. [CrossRef]

10. Evans, H.T., Jr. The molecular structure of the isopoly complex ion, decavanadate ($V_{10}O_{28}{}^{6-}$). *Inorg. Chem.* **1996**, *5*, 967–977. [CrossRef]

11. Bošnjaković-Pavlović, N.; Prevost, J.; Spasojević-de Biré, A. Crystallographic Statistical Study of Decavanadate Anion Based-Structures: Toward a Prediction of Noncovalent Interactions. *Cryst. Growth Des.* **2011**, *11*, 3778–3789. [CrossRef]

12. Chatkon, A.; Chatterjee, P.B.; Sedgwick, M.A.; Haller, K.J.; Crans, D.C. Counterion affects interaction with interfaces: The antidiabetic drugs metformin and decavanadate. *Eur. J. Inorg. Chem.* **2013**, *2013*, 1859–1868. [CrossRef]

13. Kumagai, H.; Arishima, M.; Kitagawa, S.; Ymada, K.; Kawata, S.; Kaizaki, S. New hydrogen bond-supported 3-D molecular assembly from polyoxovanadate and tetramethylbiimidazole. *Inorg. Chem.* **2002**, *41*, 1989–1992. [CrossRef] [PubMed]

14. Correia, I.; Avecilla, F.; Marcão, S.; Pessoa, J.C. Structural studies of decavanadate compounds with organic molecules and inorganic ions in their crystal packing. *Inorg. Chim. Acta* **2004**, *357*, 4476–4487. [CrossRef]

15. Samart, N.; Saeger, J.; Haller, K.J.; Aureliano, M.; Crans, D.C. Interaction of decavanadate with interfaces and biological model membrane systems: Characterization of soft oxometalate systems. *J. Mol. Eng. Mater.* **2014**, *2*, 1–21. [CrossRef]

16. Aureliano, M.; Gândara, R.M. Decavanadate effects in biological systems. *J. Inorg. Biochem.* **2005**, *99*, 979–985. [CrossRef] [PubMed]

17. Da Silva, J.L.F.; da Piedade, M.F.M.; Duarte, M.T. Decavanadates: A building-block for supramolecular assemblies. *Inorg. Chim. Acta* **2003**, *356*, 222–242. [CrossRef]

18. Kasuga, N.C.; Umeda, M.; Kidokoro, H.; Ueda, K.; Hattori, K.; Yamaguchi, K. Four novel solid-state supramolecular assemblies constructed from decavanadate salts and decamethylcucurbit[5]uril. *Cryst. Growth Des.* **2009**, *9*, 1494–1498. [CrossRef]

19. Schulz-Dobrick, M.; Jansen, M. Structure-directing effects in the supramolecular intercluster compound [$Au_9(PPh_3)_8$]$_2$[$V_{10}O_{28}H_3$]$_2$: Long-range *versus* short-range bonding interactions. *Inorg. Chem.* **2007**, *46*, 4380–4382. [CrossRef] [PubMed]

20. Román, P.; Aranzabe, A.; Luque, A.; Gutiérrez-Zorrilla, J.M.; Martínez-Ripoll, M. Effects of protonation in decavanadates: Crystal structure of tetrakis (n-hexylammonium) dihydrogendecavanadate (V). *J. Chem. Soc. Dalton Trans.* **1995**, *13*, 2225–2231. [CrossRef]

21. Arrieta, J.M.; Amigo, J.M.; Gili, P. Crystal data for the decavanadates of 2, 4-, 3, 4-, and 3, 5-dimethylpyridine and 2, 4, 6-trimethylpyridine. *J. Appl. Cryst.* **1981**, *14*, 472–473. [CrossRef]

22. Lv, Y.K.; Jiang, Z.G.; Gan, L.H.; Liu, M.X.; Feng, Y.L. Three novel organic-inorganic hybrid materials based on decaoxovanadates obtained from a new liquid phase reaction. *CrystEngComm* **2012**, *14*, 314–322. [CrossRef]

23. Sánchez-Lara, E.; Sánchez-Lombardo, I.; Pérez-Benítez, A.; Mendoza, Á.; Flores-Álamo, M.; Vergara, E.G. A New Dicationic Ring [(Water)$_6$–(Ammonium)$_2$] Acts as a Building Block for a Supramolecular 3D Assembly of Decavanadate Clusters and 4-(*N*, *N*-dimethylamino)pyridinium Ions. *J. Clust. Sci.* **2015**, *26*, 901–912. [CrossRef]

24. Nilsson, J.; Nordlander, E.; Behrens, U.; Rehder, D. Hexakis(tetraaquasodium) decavanadate(V) dihydrate. *Acta Cryst.* **2010**, *66*, i30–i31. [CrossRef] [PubMed]

25. Fratzky, D.; Schneider, M.; Rabe, S.; Meisel, M. (NH_4)$_4$$Na_2$[$V_{10}O_{28}$]·$10H_2O$. *Acta Cryst.* **2010**, *56*, 740–741. [CrossRef]

26. Wu, B.; Xu, X.; Chen, K.; Xiao, Z.; Wu, P. Crystal structure of hexakis(4-(dimethylamino)pyridin-1-ium) decavanadate-water (1:16), $C_{42}H_{98}N_{12}O_{44}V_{10}$. *Z. Kristallogr.* **2015**, *230*, 353–355. [CrossRef]

27. Spek, A.L. Single-crystal structure validation with the program PLATON. *J. Appl. Cryst.* **2003**, *36*, 7–13. [CrossRef]

28. Macrae, C.F.; Bruno, I.J.; Chisholm, J.A.; Edgington, P.R.; McCabe, P.; Pidcock, E.; Wood, P.A. Mercury CSD 2.0–new features for the visualization and investigation of crystal structures. *J. Appl. Cryst.* **2008**, *41*, 466–470. [CrossRef]

29. Adams, S. SOFTBV. Version 0.96. 2004. Available online: http://www.softbv.net/ (accessed on 31 March 2016).

30. Sinnokrot, M.O.; Sherrill, C.D. Substituent effects in π-π interactions: Sandwich and T-shaped configurations. *J. Am. Chem. Soc.* **2004**, *126*, 7690–7697. [CrossRef] [PubMed]

31. Bryant, G.L.; King, J.A. Structures of two acylpyridinium salts and one simple pyridinium salt. *Acta Cryst.* **1992**, *48*, 2036–2039. [CrossRef]

32. Chao, M.; Schempp, E.; Rosenstein, D. 4-Dimethylaminopyridine hydrochloride dihydrate. *Acta Cryst.* **1997**, *33*, 1820–1823. [CrossRef]

33. Vembu, N.; Nallu, M.; Garrison, J.; Youngs, W.J. 4-Dimethylaminopyridinium picrate: Supramolecular aggregation through extensive N—H···O and C-H···O interactions. *Acta Cryst.* **2003**, *59*, o913–o916. [CrossRef]

34. Mustaqim, R.M.; Ali, S.; Razak, I.A.; Fun, H.K.; Goswami, S.; Adak, A. 4-(N, N-Dimethylamino) pyridinium perchlorate. *Acta Cryst.* **2005**, *61*, o3733–o3734. [CrossRef]

35. Groom, C.R.; Allen, F.H. The Cambridge Structural Database in retrospect and prospect. *Angew. Chem. Int. Ed.* **2014**, *53*, 662–671. [CrossRef] [PubMed]

36. Zavalij, P.Y.; Chirayil, T.; Whittingham, M.S. Crystal structure of tetrasodium bis (tetramethylammonium) decavanadate icosahydrate, $Na_4(N(CH_3)_4)_2(V_{10}O_{28})(H_2O)_{20}$. *Z. Krist.-New Cryst.* **1997**, *212*, 321–322.

37. Liu, H.; Wang, J.; Li, Y.; Jian, F. Synthesis and Crystal Structure of the Heteronuclear Decavanadates Complex: $[Fe(phen)_3]_2 \cdot [V_{10}O_{28}] \cdot 15H_2O$. *J. Chem. Crystallogr.* **2011**, *41*, 1254–1257. [CrossRef]

38. Etter, M.C. Encoding and decoding hydrogen-bond patterns of organic compounds. *Acc. Chem. Res.* **1990**, *23*, 120–126. [CrossRef]

39. Motherwell, W.S.; Shields, G.P.; Allen, F.H. Automated assignment of graph-set descriptors for crystallographically symmetric molecules. *Acta Cryst.* **2000**, *56*, 466–473. [CrossRef]

40. Gómez-Saiz, P.; García-Tojal, J.; Maestro, M.A.; Arnaiz, F.J.; Rojo, T. Evidence of desulfurization in the oxidative cyclization of thiosemicarbazones. Conversion to 1, 3, 4-oxadiazole derivatives. *Inorg. Chem.* **2002**, *41*, 1345–1347. [CrossRef] [PubMed]

41. Chaplin, M. Water Absoption Spectrum. Available online: http://www1.lsbu.ac.uk/water/water_vibrational_spectrum.html. (accessed on 12 May 2016).

42. Ben Nasr, M.; Lefebvre, F.; Ben Nasr, C. Synthesis, Crystal Structure and Infrared Characterization of Bis(4-dimethlyamino-pyridinium) Tetrachlorocuprate. *Am. J. Anal. Chem.* **2015**, *6*, 446–456. [CrossRef]

43. Sundaraganesan, N.; Kalaichelvan, S.; Meganathan, C.; Joshua, B.D.; Cornard, J. FT-IR, FT-Raman spectra and ab initio HF and DFT calculations of 4-*N,N′*-dimethylamino pyridine. *Spectrochim. Acta A* **2008**, *71*, 898–906. [CrossRef] [PubMed]

44. Koleva, B.B.; Kolev, T.; Seidel, R.W.; Tsanev, T.; Mayer-Figge, H.; Spiteller, M.; Sheldrick, W.S. Spectroscopic and structural elucidation of 4-dimethylaminopyridine and its hydrogensquarate. *Spectrochim. Acta A* **2008**, *71*, 695–702. [CrossRef] [PubMed]

45. Frost, R.L.; Erickson, K.L.; Weier, M.L.; Carmody, O. Raman and infrared spectroscopy of selected vanadates. *Spectrochim. Acta A* **2005**, *61*, 829–834. [CrossRef] [PubMed]

46. Wery, A.S.; Gutierrez-Zorrila, J.M.; Luque, A.; Roman, P.; Martinez-Ripoll, M. Influence of protonation on crystal packing and thermal behaviour of tert-butylammonium decavanadates. *Polyhedron* **1996**, *15*, 4555–4564. [CrossRef]

47. Omri, I.; Mhiri, T.; Graia, M. Novel decavanadate cluster complex $(HImz)_{12}(V_{10}O_{28})_2 \cdot 3H_2O$: Synthesis, characterization, crystal structure, optical and thermal properties. *J. Mol. Struct.* **2015**, *1098*, 324–331. [CrossRef]

48. Frost, R.L.; Palmer, S.J. Raman spectroscopic study of pascoite $Ca_3V_{10}O_{28} \cdot 17 H_2O$. *Spectrochim. Acta A* **2011**, *78*, 248–252. [CrossRef] [PubMed]

49. Havelková, A.; Tatiersky, J. Preparation, chemical characterization and thermal behaviour of some alkyldiammonium polyoxovanadates (V). *Thermochim. Acta* **1999**, *329*, 67–71.

50. Ulická, Ľ.; Vargová, Č. Thermal analysis of some double decavanadates. *Chem. Zvesti* **1973**, *27*, 152–158. Available online: http://www.chempap.org/file_access.php?file=272a152.pdf (accessed on 6 April 2016).

51. Ulická, Ľ. Thermal decomposition of decavanadates of bivalent metals. *J. Therm. Anal.* **1980**, *18*, 127–136.

52. Sheldrick, G.M. Crystal structure refinement with SHELXL. *Acta Cryst.* **2015**, *71*, 38.

53. Unpublished results from our current research.